AJNR

Parent Vessel Size and Curvature Strongly Influence Risk of Incomplete Stent Apposition in Enterprise Intracranial Aneurysm Stent Coiling

R.S. Heller and A.M. Malek

AJNR Am J Neuroradiol 2011, 32 (9) 1714-1720
doi: https://doi.org/10.3174/ajnr.A2584
http://www.ajnr.org/content/32/9/1714

ORIGINAL RESEARCH

Parent Vessel Size and Curvature Strongly Influence Risk of Incomplete Stent Apposition in Enterprise Intracranial Aneurysm Stent Coiling

R.S. Heller
A.M. Malek

BACKGROUND AND PURPOSE: Flexible microstents, such as the closed-cell EN, have facilitated adjunctive coiling of intracranial aneurysms. Little data are available on the ability of the stent struts to maintain vessel-wall apposition once deployed in the tortuous cerebral vasculature and the prevalence of ISA. The purpose of this study was to evaluate the relationship between geometric features of the parent vessel at the stent deployment site and prevalence of ISA.

MATERIALS AND METHODS: Postprocedural 3T-MRA was performed in a cohort of 39 patients undergoing EN stent-assisted intracranial aneurysm coiling. 3T-MRA was analyzed for the presence of ISA and supplemented by angiographic C-arm FPCT (DynaCT). Parent vessel diameter, curvature radius, and stent-subtended arc angle were measured at the site of deployment and analyzed for prediction of ISA in the ICA.

RESULTS: 3T-MRA uncovered a unique crescent flow pattern (CS) outside the EN struts, which was confirmed by FPCT to indicate ISA resulting from EN crimping. ISA was detected on 3T-MRA in 19/39 patients (49%). Univariate analysis revealed ISA in the ICA to correlate with a large stent-subtended angle, a small curvature radius, and a large diameter but not stent length or jailing versus a sequential technique. Multivariate analysis identified ISA to correlate with vessel-curvature radius (OR, 253; $P = .009$), stent-subtended angle (OR, 225; $P = .005$), and parent vessel diameter (OR, 8.49; $P = .044$).

CONCLUSIONS: In this study, ISA was detectable by 3T-MRA in a significant proportion of patients undergoing EN stent-assisted coiling of ICA aneurysms in a vessel geometry– and stent-deployment location–dependent manner. This characteristic of EN coiling at this potentially tortuous location should be taken into account when selecting an endovascular strategy.

ABBREVIATIONS: CS = crescent sign; CS+ = CS present; CS– = CS absent; 3D-RA = 3D rotational angiography; DSA = digital subtraction angiography; EN = Enterprise stent or vascular reconstruction device; FPCT = flat panel CT; ICA = internal carotid artery; ISA = incomplete stent apposition; MPR = multiplanar reformation; OR = odds ratio; 3T-MRA = 3T time-of-flight MR angiography

Endovascular embolization using a stent-assisted technique has proved to be an effective option in the treatment of wide-neck intracranial aneurysms.[1-4] Stents serve as a physical barrier to prevent coil protrusion into the parent vessel during coiling of wide-neck or fusiform lesions. Follow-up imaging of patients who have undergone stent-mediated coil embolization procedures has traditionally focused on the presence or absence of residual filling in the dome.[5] Despite excellent laboratory evaluations of stent conformation in vitro,[6,7] data on visualization and strut configuration of stents deployed in the intracranial circulation remain scant. Several studies have evaluated the architecture of stents within coronary vessels and have noted the presence of ISA to the vessel wall.[8-10] Because this finding may be associated with adverse clinical events such as late stent thrombosis[10,11] in the coronary circulation, we sought to identify the presence of any ISA within the intracranial circulation in patients undergoing stent-mediated coiling by using the self-expanding intracranial EN (Cordis, Miami Lakes, Florida). Correlating our findings with angiographic FPCT, we describe here a new crescent-shaped flow signal intensity external to the stent struts on 3T-MRA as a marker for ISA in EN-treated aneurysms and describe the morphologic characteristics of target vessels that predispose to poor stent–vessel wall apposition.

Received December 5, 2010; accepted after revision February 7, 2011.

From the Cerebrovascular and Endovascular Division, Departments of Neurosurgery and Radiology, Tufts Medical Center and Tufts University School of Medicine, Boston, Massachusetts.

Please address correspondence to Adel M. Malek, MD, PhD, Tufts Medical Center, 800 Washington St, Proger 7, Boston, MA 02111; e-mail: amalek@tuftsmedicalcenter.org

http://dx.doi.org/10.3174/ajnr.A2584

Materials and Methods

Patient Selection

Since January 2009, all patients undergoing stent-mediated coiling in our service have routinely undergone prospective 3T-MRA postprocedurally. All aneurysm stent-coiling procedures using ENs in the intracranial vasculature from January 2009 to September 2010 with 3T-MRA performed within 3 days of stent deployment, totaling 33 cases, were included. An additional 6 patients who underwent prospective 3T-MRA imaging within 3 days of EN deployment between June 2007 and September 2008, as part of a pilot study on the utility of 3T-MRA in randomly selected patients following stent-coiling, were also included in the study. Cases of off-label use of ENs such as the waffle-cone technique[12] were not included. The use of the EN and the current study were approved by the institutional review board.

Embolization Procedure

Patients were pretreated with clopidogrel (75 mg by mouth daily) and aspirin (325 mg by mouth daily) for at least 3 days before the proce-

dure. Stent-mediated coiling by using the EN (4.5 mm diameter by 14, 22, 28, or 37 mm length) was performed according to the manufacturer's instructions for use via a Prowler Plus Select 0.021-inch microcatheter (Codman Neurovascular, Raynham, Massachusetts). Stent coiling was performed either by using the sequential or jailing technique. In the former, the EN is first deployed, and then a separate 0.014-inch microcatheter (Excelsior SL-10; Boston Scientific, Natick, Massachusetts) is used to catheterize the aneurysm dome through the stent interstices followed by coiling. In the jailing technique, the aneurysm is first selected by the SL-10 coiling microcatheter, followed by EN deployment, thereby pinning the coiling microcatheter between the stent and vessel wall while coiling proceeds. The stent was deployed by stabilizing the delivery microwire and then unsheathing the stent by withdrawal of the Prowler Plus Select microcatheter. All patients were treated with intravenous anticoagulation for a target partial thromboplastin time of 55–70 seconds for 24 hours following the procedure.

Angiographic Analysis and MR Imaging Methods

A single calibrated flat-panel biplanar DSA system (Artis; Siemens, Erlangen, Germany) was used for all procedures. 3D-RA and angiographic C-arm FPCT were performed (DynaCT; Siemens) during the embolization procedure. Acquisitions were reconstructed and analyzed by using the Leonardo software package (Siemens).

Patients underwent 3T-MRA of the brain within 3 days of the initial procedure by using a 3T Achieva unit (Philips Healthcare, Best, the Netherlands). MRA was performed by using a 3D time-of-flight technique with a TR of 25 ms, TE of 3.45 ms, flip angle of 20°, FOV of 20 cm, with 1-mm phase-encoding, reconstructed to 512 × 512 (voxel size 0.39 × 0.39 × 0.5 mm). The volumetric 3D datasets obtained from 3T-MRA and FPCT source images were visualized in 3D by using 3D MPR and maximal intensity projection by using OsiriX software (64-bit, Version 3.8; Pixmeo, Bernex, Switzerland).

Morphologic Feature Measurement

The measurements of the morphologic features were performed in 3D by using MPR of the 3D volumetric dataset obtained from the 3D reconstruction of the post–stent deployment or post–stent coiling rotational angiographic runs. The 3D volumetric dataset was exported from the workstation and analyzed by using MPR visualization by using Osirix. The radius of curvature was measured as a feature of the parent vessel in which the stent was deployed by obtaining the radius of a circle fitted through the centerline of the carotid artery curved segment. The parent vessel diameter was measured as the average of the diameter at the distal and proximal stent-deployment sites. The stent-subtended arc angle, measured independent of the radius of vessel curvature, was evaluated on the basis of the angle at which the stent was deployed in the parent vessel.

Morphologic feature measurements were made individually and independently by both authors in a blinded fashion (without knowledge of ISA status), on separate occasions, and on different computers by using the same datasets. The interobserver correlation coefficient r values for vessel curvature, stent-subtended angle, and vessel diameter were each >.90. Values reported for each sample point are averages of each observer's measurements.

Statistical Analysis

The differences in characteristics between subtypes were evaluated by using 1-way analysis of variance, stepwise-regression modeling, χ^2 testing, and ORs for categoric values by using JMP, Version 8 (SAS, Cary, North Carolina). Statistical significance was assumed for $P < .05$.

Results

Detection of ISA by 3T-MRA

During surveillance imaging in a number of EN stent-mediated aneurysm embolization procedures in which stent positioning was thought to be paramount, high-resolution FPCT imaging was performed and evaluated for the quality of stent apposition to the vessel wall (Fig 1). In a number of patients in whom ENs were deployed around curved segments of the ICA (Fig 1), the stent exhibited central crimping and ovalization with luminal loss and the outer and/or inner stent struts were noted not to be in contact with the vessel wall, resulting in significant ISA. FPCT imaging with and without dilute contrast injection demonstrated flow of blood outside the confines of the stent lattice. Comparison and correlation of these FPCT findings were made with post-treatment 3T-MRA thin-section MPR reconstructions, which consistently revealed that the site of ISA on FPCT corresponded to a characteristic 3T-MRA flow pattern of high signal intensity outside the stent struts (Fig 1*C*). This finding was dubbed CS on the basis of its unique crescent shape (Fig 2*G* and *H*).

Analysis of 3T-MRA in EN-treated aneurysms detected the presence of CS as an indicator of ISA in 19 of 39 patients (49%). Patient subsets with and without CS were statistically indistinguishable with respect to age (60.5 ± 8.0 years and 54.9 ± 10.6 years, respectively, $P = .076$) and sex (4 men/15 women; and 3 men/17 women, respectively, $P = .622$). Lengths of ENs (14, 22, 28, and 37 mm) used in the CS+ population ($n = 0$, 17, 1, and 1) were not statistically different ($P = .122$) than those in the CS− population ($n = 1$, 14, 5, and 0). Similarly, a jailing technique was used in 17 of 19 in patients with CS compared with 16 of 20 in those with CS− ($P = .408$). Of the 19 cases demonstrated to harbor CS, 18 were located in the intracranial ICA and 1, in the middle cerebral artery. Of the 20 cases without CS, 14 were located in the ICA, 3 in the anterior communicating artery, 2 in the basilar artery, and 1 in the middle cerebral artery.

Internal Carotid Parent Vessel Characteristics Related to ISA

To determine factors contributing to ISA, we analyzed shape features of the parent vessel with respect to the deployed stent (Fig 3). Figure 3*B* demonstrates 2 stent configurations used to treat the same aneurysm, in which 2 different stent-subtended arc angles are obtained for the same radius of vessel curvature. Statistical analysis of morphologic features was limited to the 32 cases with stents deployed in the ICA to avoid biasing of results by the uneven distribution of the deployment location among cases with and without CS, given the inherent variation of vessel size and anatomy in the cerebral circulation. Among the 32 ICA cases, 18 demonstrated the CS on 3T-MRA (56%). Univariate analysis (Tables 1 and 2) for correlation of the CS revealed the radius of curvature to be significantly lower ($P = .002$) in patients with the CS (signifying a tighter curve). Similarly, parent vessel diameter was greater in patients with the CS ($P = .043$), as was the angle α subtended by the deployed

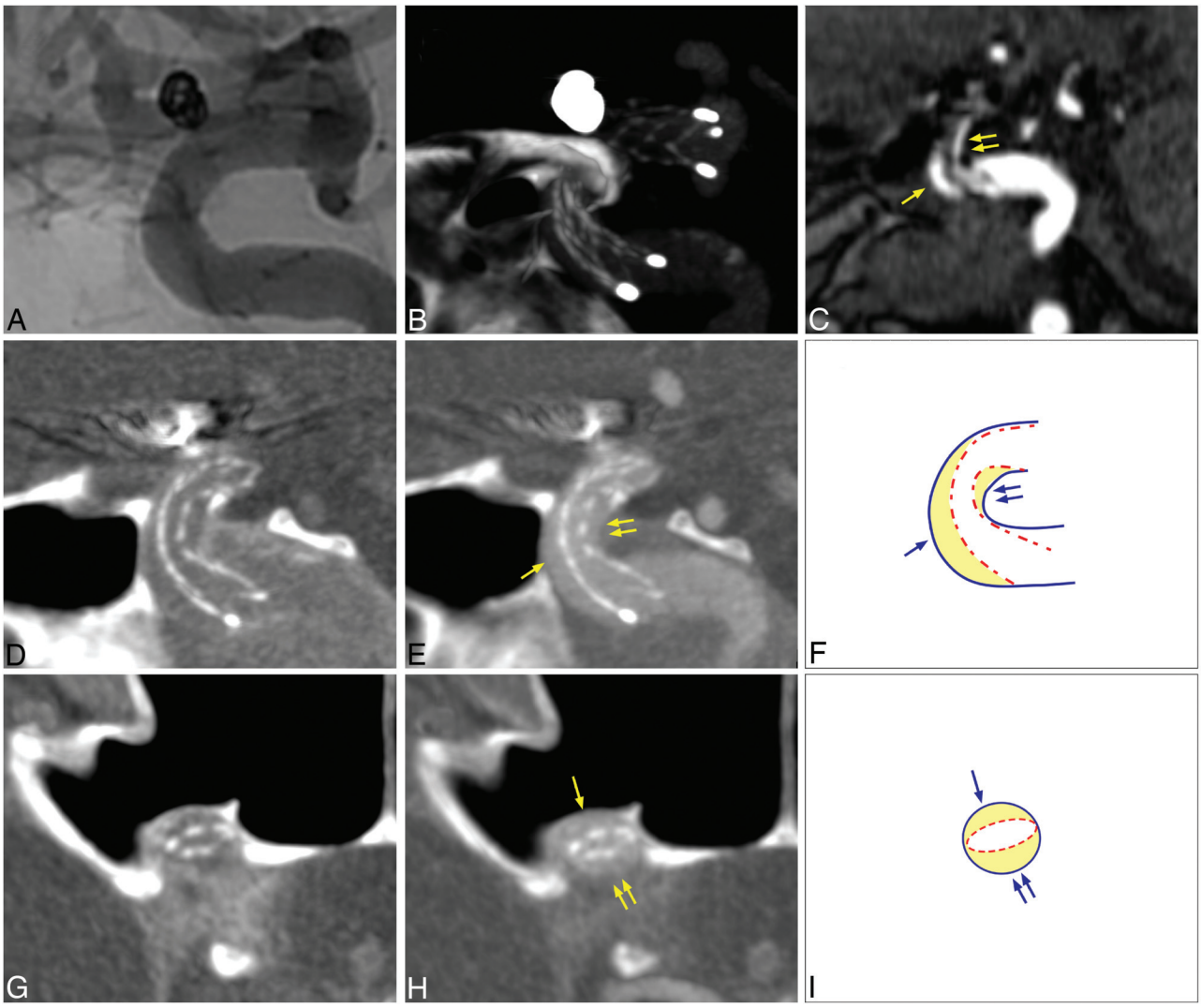

Fig 1. ISA is seen with CS in a 63-year-old woman following EN—mediated coiling of a carotid ophthalmic aneurysm. *A*, Unsubtracted digital angiography and *B*, corresponding thick-section FPCT identify the coil mass and stent crimp at the carotid siphon. *C*, CS on thin-section sagittal 3T-MRA reveals ISA on the outer (*arrow*) and inner (*double arrows*) vessel curve. *D—I*, Thin-section FPCT in sagittal (*D* and *E*) and axial (*G* and *H*) projections without (*D* and *G*) and with (*E* and *H*) dilute contrast identifies stent crimp and ISA corresponding to the CS. Schematic illustrations in sagittal (*F*) and axial (*I*) projections highlight the relative position of the stent (dashed red), parent vessel, and orphaned regions of ISA (yellow).

EN ($P < .001$). Aneurysm size was also found to have no effect on this phenomenon ($P = .546$); endovascular technique (jailing versus sequential) was similarly not different ($P = .427$).

Multivariate analysis (Table 2) by using univariate significant factors ($P < .05$) for modeling ISA was performed by using the parent vessel diameter, the parent vessel radius of curvature, and the stent-subtended angle. Multivariate logistic regression yielded an area under curve of 0.9316 in the receiver-operating characteristic, with a sensitivity of 100% and a specificity of 85% with the highest significance for the vessel radius of curvature (OR, 253; $P = .009$), followed by the stent-subtended angle (OR, 225; $P = .005$) and vessel diameter (OR, 8.49; $P = .044$).

Discussion

ISA has been defined by Rathore et al[8] as the "separation of one or more stent struts from the underlying vessel wall and observation of blood speckles between the stent struts and the vessel wall," as demonstrated with the use of intravascular sonography for visualization of the stent-containing vessel. By confirming our findings by using FPCT imaging, which has been shown to be effective in the visualization of in vivo stents,[13,14] we demonstrated the same blood flow phenomenon between the stent struts and the vessel wall by using the presence of the CS on 3T-MRA imaging. Univariate and multivariate results from this study demonstrate that following deployment of closed-cell design ENs in the intracranial ICA, ISA is more likely to be found in vessels with more tortuous anatomy.

Prior studies evaluating ISA in balloon-mounted stents deployed for coronary atherosclerosis have identified predictors of ISA to include atherosclerotic lesion length,[15] use of drug-eluting stents, unstable angina, and the absence of diabetes.[16] The significant differences in properties between balloon-mounted coronary stents and the low-radial-force self-expanding ENs make ISA etiology comparison between the 2 less compelling. EN consists of a self-expanding closed-cell design, which is significantly less stiff and has thinner struts than balloon-mounted variants.

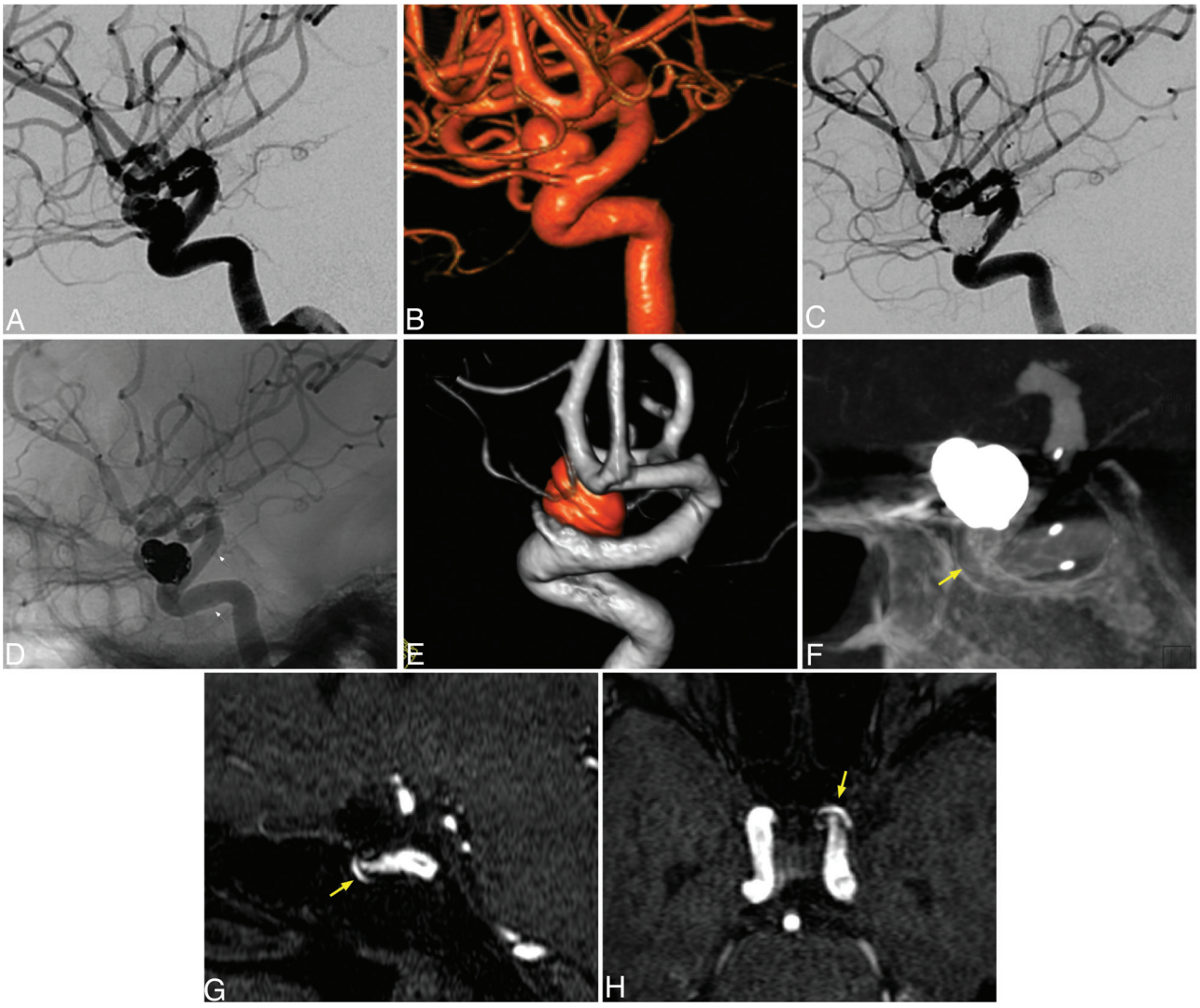

Fig 2. CS revealed in a 59-year-old woman with a wide-neck left carotid ophthalmic aneurysm. *A–D*, Lateral DSA (*A*), a 3D-RA reconstructed model (*B*), a postembolization lateral DSA (*C*), and an unsubtracted lateral digital angiogram show strut ends of the deployed 4.5 × 22 mm EN (*D*, *arrows*). *E* and *F*, Postembolization 3D-RA model (*E*) and FPCT reveal stent crimp at the siphon and an outer crescent region of ISA (*F*, *arrow*). *G* and *H*, Sagittal (*G*) and axial (*H*) 3T-MRA shows CS (*arrow*).

The clinical impact of ISA in the coronary vasculature remains under debate. Onizuka et al[17] demonstrated that no adverse clinical events occurred in 15 patients found to harbor ISA following carotid artery angioplasty and stent placement with a mean follow-up of 11 months. The RAVEL trial[18] demonstrated no adverse events in patients found to harbor ISA with a follow-up of 12 months. Other studies evaluating the long-term consequences of ISA have highlighted a significant risk. Hoffmann et al[19] described a higher incidence of myocardial infarction in patients with ISA after 4 years of follow-up compared with patients without ISA. Siqueira et al[10] performed follow-up on patients for a mean of 29 months and observed an increased incidence of stent thrombosis in patients with ISA. Cook et al[20] reported similar results, finding that patients presenting with stent thrombosis after a minimum of 12 months following stent deployment had a higher incidence of ISA. In their review of the coronary literature and the aforementioned studies, Rathore et al[8] concluded that a definite relationship existed between ISA and stent thrombosis, though they conceded that longer follow-up is necessary to elucidate the true consequences of ISA. Because the coronary stents evaluated in these previous studies are balloon-mounted and constructed of thicker and stiffer stent struts, the results elucidated in these studies in patients with coronary atherosclerosis cannot be easily correlated to stent-mediated aneurysm coiling by using self-expanding flexible stents deployed in healthier nonstenosed vessel segments.

The finding of prevalent ISA in tightly curved vessels may be a direct result of the closed-cell design of the EN. Although the closed-cell design is advantageous at serving as a smooth interface at the aneurysm neck to act as scaffolding for coil deployment, our results point to this design as an inherent limitation in tortuous vessels having small curvature radius. In addition, the higher propensity for the EN to demonstrate ISA in larger diameter vessels suggests that the stent lacks outer radial force to sufficiently appose the wall near its deployment diameter. The EN may be better suited for use in smaller caliber vessels if significant curvature exists. If the vessel diameter is close to 4.0 mm, then the EN may be better limited to straight-vessel segments because its use in larger curved vessels

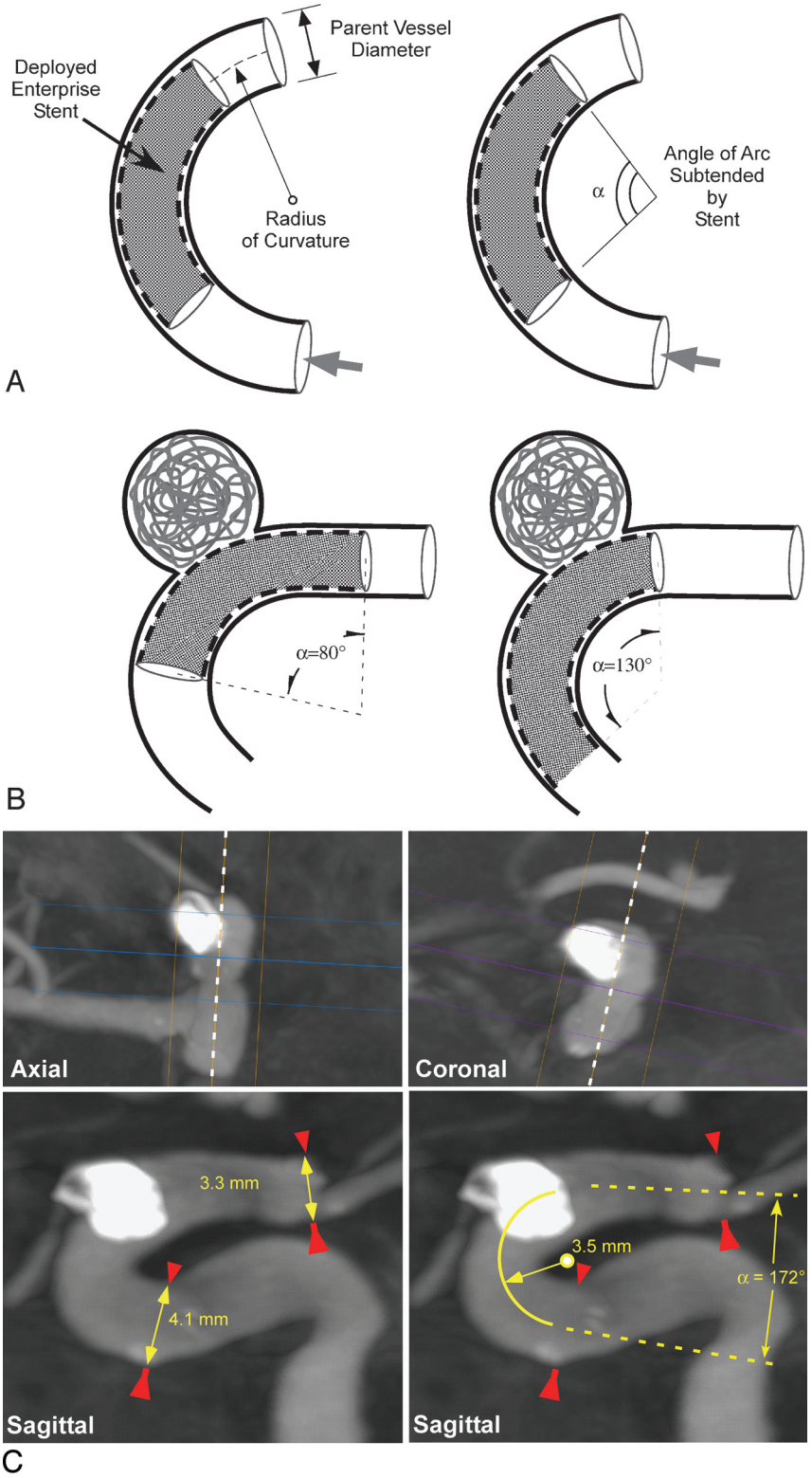

Fig 3. Schematic showing measured parent vessel parameters in the stented segment including the parent vessel diameter and the radius of curvature, which are functions of the underlying parent vessel geometry. *A*, The angle of the arc subtended by the deployed stent is measured independently and is a function of the location of the stent within the vessel. The stent-subtended arc angle is stent deployment location–dependent and is related to the stent landing zone with respect to the curved parent vessel. *B*, The stent-subtended angle can differ significantly even at a given location, depending on the relative stent position. *C*, 3D MPR of the 3D volumetric dataset with the axial and coronal orientations adjusted so as to enable the orthogonal visualization of the curve of the parent vessel, shown here with representative measurements. Red arrows demarcate the proximal and distal ends of the deployed EN.

could be associated with ISA. The current EN is manufactured in varying lengths but at a single uniform maximum deployed diameter of 4.5 mm. The findings presented here suggest the need for a larger EN configuration for use in vessels of near 4-mm luminal diameter. The findings suggest that 1 way to decrease ISA likelihood in ICA EN coiling may be to select a

Table 1: Univariate analysis of the dependence of ISA as detected by the presence of CS on 3T-MRA in intracranial ICA lesions

	CS+	CS−	*P* Value
Patient count with ICA lesions	18	14	
Vessel curvature radius (mm)	7.26 ± 2.0	9.8 ± 2.2	.002
Stent-subtended arc angle α	144 ± 32°	95.2 ± 42°	<.001
Parent vessel diameter (mm)	4.06 ± 0.32	3.74 ± 0.54	.043
Stent length (22, 28, 37 mm)	16:1:1	10:4:0	.125
Aneurysm size (mm)	6.99 ± 5.2	7.99 ± 3.6	.546
Technique (jailing:sequential)	16:2	11:3	.427

Table 2: Multivariate analysis of the dependence of ISA on morphologic features in intracranial ICA lesions

	χ^2	*P* Value
Vessel curvature radius	6.842	.009
Stent-subtended arc angle α	8.046	.005
Parent vessel diameter	4.062	.044
Total model	21.323	<.0001

landing zone for the stent deployment that attempts to decrease the stent-subtended angle at any given aneurysm location as suggested in Fig 3*B* (left panel instead of right), provided that this is possible without compromising the ability of the stent to mechanically scaffold the coils properly.

The presence of poor stent apposition with the EN also has at least 2 technical ramifications for subsequent endovascular intervention. In the first, the presence of struts in the center of the vessel lumen may interfere with future microcatheter navigation or the addition of concentric stent placement; worse, it may lead to stent movement during microcatheter manipulation. In the second, the lack of stent apposition to the vessel wall harboring the aneurysm neck could potentially result in unintended partial coil herniation into the parent vessel or at least a higher exposure of the coil pack to intraluminal flow.

The EN has been linked by a number of case reports to a delayed migration phenomenon in the posterior circulation, which remains poorly explained.[21-23] The poor stent apposition highlighted in curved-vessel segments adds another possible mechanism of stent migration, because the lack of stent strut contact to the vessel wall may make the already lubricious coated stent less anchored and more prone to sliding. Nonetheless, the current study is predominantly in the anterior circulation and may, therefore, be of limited relevance to the cases of migration, which were in the posterior circulation. ISA, however, also increases the surface area of the stent within the vessel lumen, thereby exposing the stent to the central high-flow velocities expected in the approximately parabolic velocity profile in the target vessels. Although such greater exposure would increase the hemodynamic drag on the stent, it is not likely to explain the reported cases of migration, which led to proximal, not distal, delayed movement of the deployed EN.

Etiologically, the crescent-shaped 3T time-of-flight MR imaging signal intensity in tightly curved vessels with ISA may be directly related to the curved nature of the artery and the less curved nature of the closed-cell design EN. Measurements of the volume of the CS by using summation of the 3T-MRA signal intensity as a potential proportional indicator of ISA severity did not demonstrate a linear relationship to the morphologic features reported in the study (data not shown). It is likely that the 3T-MRA CS is not linearly proportional to the degree of ISA and may be best used as a binary indicator. This is possibly the result of the relatively low spatial resolution of MR imaging and of metal artifact signal-intensity dropoff from the stent struts. Both could lead to the inability of 3T-MRA to sufficiently delineate the small margins of the CS area. A comparison of the crescentic area of ISA in Figs 1 and 2 between 3T-MRA CS and the corresponding FPCT images also confirms the lower spatial resolution of 3T-MRA. These limitations of MR imaging suggest that the true degree of less severe ISA may be underestimated and may be even higher than that reported in the current study. A more detailed quantitative analysis of the area and shape of the ISA would likely necessitate the use of FPCT for computation of the orphaned volume in the zone of ISA.

In light of the link between vessel anatomy, relative stent-deployment location, and development of ISA in the ICA, we recommend that use of closed-cell design ENs be reserved for vessels with narrower diameters and larger radii of curvature. Preferential selection of these vessels may promote a lower likelihood of stent malapposition and a more favorable deployed-stent architecture. Given the significant lack of stent-vessel wall apposition at vessel diameters close to 4.0 mm, stent-subtended arc angles >100°, and tight vessel curvature, procedures requiring stent deployment in tortuous intracranial locations such as the carotid siphon warrant careful analysis. The current findings may also be relevant to recent attempts to employ the EN for the treatment of intracranial atherosclerosis because these suggest that it may be better suited for straight rather than curved segments.[24]

Conclusions

The central finding of this study is that the closed-cell design EN is susceptible to malapposition to the vessel wall when deployed in vessels with tortuous anatomy. This phenomenon can be detected by the use of the CS on 3T-MRA. Careful preprocedural morphologic analysis is warranted to select vessels that will be less likely to induce incomplete stent apposition. Further work is needed to evaluate the long-term consequences of incomplete stent apposition of ENs in the cerebral vasculature

Disclosures: Adel M. Malek, *Research Support (including provision of equipment or materials)*: Boston Scientific and Codman Neurovascular, *Details*: Unrestricted research grants on topics not directly related to the topic in manuscript. *Speaker Bureau:* Boston Scientific, *Details*: Presented at scientific symposia (total <$10,000)

References

1. Wells-Roth D, Biondi A, Janardhan V, et al. **Endovascular procedures for treating wide-necked aneurysms.** *Neurosurg Focus* 2005;18:E7
2. Phatouros CC, Sasaki TY, Higashida RT, et al. **Stent-supported coil embolization: the treatment of fusiform and wide-neck aneurysms and pseudoaneurysms.** *Neurosurgery* 2000;47:107–13, discussion 113–15
3. Lee YJ, Kim DJ, Suh SH, et al. **Stent-assisted coil embolization of intracranial wide-necked aneurysms.** *Neuroradiology* 2005;47:680–89
4. Irie K, Negoro M, Hayakawa M, et al. **Stent assisted coil embolization: the treatment of wide-necked, dissecting, and fusiform aneurysms.** *Interv Neuroradiol* 2003;9:255–61
5. Sedat J, Chau Y, Mondot L, et al. **Endovascular occlusion of intracranial wide-necked aneurysms with stenting (Neuroform) and coiling: mid-term and long-term results.** *Neuroradiology* 2009;51:401–09
6. Benndorf G, Claus B, Strother CM, et al. **Increased cell opening and prolapse of**

struts of a Neuroform stent in curved vasculature: value of angiographic computed tomography—technical case report. *Neurosurgery* 2006;58:ONS-E380, discussion ONS-E380
7. Ebrahimi N, Claus B, Lee CY, et al. **Stent conformity in curved vascular models with simulated aneurysm necks using flat-panel CT: an in vitro study.** *AJNR Am J Neuroradiol* 2007;28:823–29
8. Rathore S, Terashima M, Habara M, et al. **Incomplete stent apposition after coronary stent implantation: myth or reality?** *J Interv Cardiol* 2009;22:341–49
9. Radu M, Jorgensen E, Kelbaek H, et al. **Strut apposition after coronary stent implantation visualised with optical coherence tomography.** *EuroIntervention* 2010;6:86–93
10. Siqueira DA, Abizaid AA, Costa Jde R, et al. **Late incomplete apposition after drug-eluting stent implantation: incidence and potential for adverse clinical outcomes.** *Eur Heart J* 2007;28:1304–09
11. Zhang F, Qian J, Ge J. **Coexistent in-stent restenosis, late incomplete stent apposition and mural thrombus in a zotarolimus-eluting stent.** *J Invasive Cardiol* 2008;20:423–25
12. Horowitz M, Levy E, Sauvageau E, et al. **Intra/extra-aneurysmal stent placement for management of complex and wide-necked- bifurcation aneurysms: eight cases using the waffle cone technique.** *Neurosurgery* 2006;58:ONS-258–262, discussion ONS-262
13. Namba K, Niimi Y, Song JK, et al. **Use of Dyna-CT angiography in neuroendovascular decision-making: a case report.** *Interv Neuroradiol* 2009;15:67–72. Epub 2009 Apr 15
14. Nemes B, Lukacs L, Balazs G, et al. **High-resolution CT and angiographic evaluation of NexStent wall adaptation.** *Cardiovasc Intervent Radiol* 2009;32:436–40
15. Weissman NJ, Ellis SG, Grube E, et al. **Effect of the polymer-based, paclitaxel-eluting TAXUS Express stent on vascular tissue responses: a volumetric intravascular ultrasound integrated analysis from the TAXUS IV, V, and VI trials.** *Eur Heart J* 2007;28:1574–82. Epub 2007 May 31
16. Tanabe K, Serruys PW, Degertekin M, et al. **Incomplete stent apposition after implantation of paclitaxel-eluting stents or bare metal stents: insights from the randomized TAXUS II trial.** *Circulation* 2005;111:900–05
17. Onizuka M, Kazekawa K, Nagata S, et al. **The significance of incomplete stent apposition in patients undergoing stenting of internal carotid artery stenosis.** *AJNR Am J Neuroradiol* 2006;27:1505–07
18. Degertekin M, Serruys PW, Tanabe K, et al. **Long-term follow-up of incomplete stent apposition in patients who received sirolimus-eluting stent for de novo coronary lesions: an intravascular ultrasound analysis.** *Circulation* 2003;108:2747–50
19. Hoffmann R, Morice MC, Moses JW, et al. **Impact of late incomplete stent apposition after sirolimus-eluting stent implantation on 4-year clinical events: intravascular ultrasound analysis from the multicentre, randomised, RAVEL, E-SIRIUS and SIRIUS trials.** *Heart* 2008;94:322–28. Epub 2007 Aug 29
20. Cook S, Wenaweser P, Togni M, et al. **Incomplete stent apposition and very late stent thrombosis after drug-eluting stent implantation.** *Circulation* 2007;115:2426–34
21. Kelly ME, Turner RD, Moskowitz SI, et al. **Delayed migration of a self-expanding intracranial microstent.** *AJNR Am J Neuroradiol* 2008;29:1959–60
22. Rodriguez GJ, Maud A, Taylor RA. **Another delayed migration of an Enterprise stent.** *AJNR Am J Neuroradiol* 2009;30:E57
23. Lavine SD, Meyers PM, Connolly ES, et al.. **Spontaneous delayed proximal migration of Enterprise stent after staged treatment of wide-necked basilar aneurysm: technical case report**. *Neurosurgery* 2009;64:E1012, discussion E1012
24. Mocco J, Hanel RA, Sharma J, et al. **Use of a vascular reconstruction device to salvage acute ischemic occlusions refractory to traditional endovascular recanalization methods.** *J Neurosurg* 112:557–62